Data Consistency Conditions for 2D Truncated Parallel Projections

Rolf Clackdoyle and Laurent Desbat

***Abstract*-- New data consistency conditions (DCC) have been derived for parallel projections in two dimensions, which have the remarkable feature that they can be applied to truncated projections. We show the derivation of these conditions and illustrate a potential application to motion detection and compensation.**

I. Introduction

In the context of image reconstruction, data consistency conditions (DCC), also called range conditions, are mathematical descriptions of the redundancies in projection measurements. These conditions can usefully decouple the tomographic reconstruction problem from other systematic effects in the measurement model. For example, if the target specimen (usually a patient in the medical imaging scenario) undergoes an abrupt rigid motion, the measurement model now consists of both a very large linear tomographic system as well as a handful of nonlinear parameters that describe the motion and the time point when the motion occurred. If DCC are available for the tomographic model, then the small number of nonlinear parameters can be estimated by requiring the adjusted model to satisfy the DCC, which is usually a far easier task than repeated reconstructions using trial nonlinear parameters. This technique has found numerous applications in various areas of medical imaging, including in x-ray CT (e.g. [Bas00, Pat02, Def03, Hsi04, Yu07, Maz10, Tan11]).

The most well-known DCC are those of Helgason-Ludwig (HL) [Lud66, Hel80], which apply to the Radon transform in parallel projection geometries. Others have been established for fanbeam, cone-beam, exponential, and attenuated transforms and for different formats such as for Fourier transformed sinograms. (For example DCC: [Jon38, Nat83, Fin83, Edh86, Agu95, Pat02, Che05, Yu06, Lev10, ClD13]). Only a few of these DCC allow subsets of a full tomographic set of data to be examined for consistency. For example, with the HL conditions, the order zero condition is that the projection sums are constant, so any number of projections can be checked for consistency of their DC terms. Similarly, any two parallel projections can will determine the degree-1 polynomial specified in the HL DCC, and other projections can then be checked against this polynomial. Convenient descriptions of DCC where subsets of projections can be checked exist in a few cases, see [ClD13] for an example using cone-beam projections. This flexibility to apply DCC to subsets of measurements increases their usefulness in applications.

With the advent of true ROI reconstruction in the plane (see [Cla10] for an overview), it is important to consider the situation of truncated projections. To our knowledge, no DCC are known to exist that can treat truncated projections, with the exception of the differential form given in [Joh30], which has the both the advantage and disadvantage of applying locally to fully 3D measurements; they cannot directly be used for just two truncated cone-beam projections for example.

We announce here what we believe to be the first DCC that can handle truncated parallel projections in the plane. We provide a simple proof of the consistency which we illustrate with simulations. We then discuss how these new DCC might be applied in practice, using a toy problem (for illustration) that involves motion detection of a known tumour-like object.

II. Theory

We let $f(x, y)$ represent the unknown density function, and $p(\phi, r)$ be the parallel projection of f defined by

$$p(\phi, r) = \int_{-\infty}^{\infty} f(r\alpha + s\beta)ds \qquad (1)$$

where $\phi \in (-\pi/2, \pi/2)$ and $\alpha = (\cos\phi, \sin\phi)$, $\beta = (-\sin\phi, \cos\phi)$. Now, for each non-negative n, we consider a weighted backprojection of $p(\phi, r)$, where the weight depends on n. The projection $p(\phi, \cdot)$ will be weighted by $\tan^n\phi / \cos\phi$ prior to backprojection. The singularity near $\pm\pi/2$ will be dealt with by only considering $|\phi| < \pi/2 - \varepsilon$ as will be discussed below, but to simplify the derivation we ignore this detail for now. The weighted backprojection is given by

$$b_n(x, y) = \int_{-\pi/2}^{\pi/2} p(\phi, (x, y) \cdot \alpha) \frac{\tan^n\phi}{\cos\phi} d\phi \qquad (2)$$

Since the system is shift-invariant, the behavior of the weighted backprojection can be completely characterized by its point response function (PRF), so we first examine this PRF, and then show how it leads to consistency conditions in the form of polynomials of degree n which can accommodate truncation of the projections.

A direct substitution of equation 1 into equation 2, followed by the substitution $s = (x, y) \cdot \beta - s'$ yields

$$b_n(x, y) = \int_{-\pi/2}^{\pi/2} \int_{-\infty}^{\infty} f(((x, y) \cdot \alpha)\alpha + s\beta) \frac{\tan^n\phi}{\cos\phi} ds d\phi \qquad (3a)$$

R. Clackdoyle is with the Laboratoire Hubert Curien, CNRS UMR 5516, Saint Etienne, France (e-mail: rolf.clackdoyle@univ-st-etienne.fr).

L. Desbat is with the TIMC-IMAG laboratory, CNRS UMR 5525, and Joseph Fourier University, Grenoble, France (e-mail laurent.desbat@imag.fr).

This work was partially supported by the Agence Nationale de la Recherche (France), project "DROITE," number ANR-12-BS01-0018.

$$= \int_{-\pi/2}^{\pi/2}\int_{-\infty}^{\infty} f((x,y)-s'\beta)\frac{\tan^n\phi}{|s'|\cos\phi}|s'|ds'd\phi \quad (3b)$$

$$= \int_{-\infty}^{\infty}\int_{-\infty}^{\infty} f((x,y)-(x',y'))\frac{(-x')^n}{(y')^n|y'|}\,dx'dy' \quad (3c)$$

$$= \int_{-\infty}^{\infty}\int_{-\infty}^{\infty} f(x-x',y-y')\;h_n(x',y')\;dx'dy' \quad (3d)$$

where the point response function is

$$h_n(x,y) = \frac{(-1)^n x^n}{y^{n+1}}\mathrm{sgn}(y) \quad (4)$$

Equation 3c was obtained from equation 3b by performing the polar-to-rectangular coordinate change of variables $(x',y') = (-s'\sin\phi, s'\cos\phi)$, with $dx'dy' = |s'|ds'd\phi$.

Note that for $n = 0$, the point response function becomes $h_0(x,y) = 1/|y|$ and the backprojection $b_0(x,y)$ is equal to an unweighted integration in the x-direction of $f(x,y)$.

We continue the derivation to arrive at our main result.

$$b_n(x,y_0) = \int_{-\infty}^{\infty}\int_{-\infty}^{\infty} f(x',y')\;h_n(x-x',y_0-y')\;dx'dy' \quad (5a)$$

$$= \int_{-\infty}^{\infty}\int_{-\infty}^{\infty} f(x',y')\;\frac{(x'-x)^n}{(y_0-y')^{n+1}}\mathrm{sgn}(y_0-y')\;dx'dy' \quad (5b)$$

$$= c_0 + c_1x + c_2x^2 + \ldots + c_nx^n \quad (5c)$$

where we consider y_0 to be held constant and c_k is given by

$$c_k = (-1)^k\binom{n}{k}\times \int_{-\infty}^{\infty}\int_{-\infty}^{\infty} f(x',y')\frac{(x')^{n-k}}{(y_0-y')^{n+1}}\mathrm{sgn}(y_0-y')dx'dy' \quad (6)$$

The new consistency conditions for 2D parallel projections can now be stated as follows:

Theorem: Suppose that a sinogram $p(\phi,r)$ satisfies equation 1 for some density function f. For y_0 chosen such that the line $y = y_0$ does not intersect the compact support of f, and for any non-negative integer n, the weighted backprojection b_n (equation 2) evaluated along the line segment $[(x_a,y_0),(x_b,y_0)]$ is a polynomial function of x, of degree at most n. That is,

$$b_n(x,y_0) = c_0 + c_1x + c_2x^2 + \ldots + c_nx^n \quad x\in[x_a,x_b] \quad (7)$$

Note that by choosing y_0 such that the line $y = y_0$ does not intersect the support of f, all potential singularities vanish. The expression for c_k given by equation 6 no longer contains a singular kernel because the support of f restricts the integration range to exclude $y = y_0$. Furthermore, with the compact support of f not touching the line $y = y_0$, we see that there must exist some small ε such that the projection of the support of f at any angles $|\phi| \in [\pi/2-\varepsilon, \pi/2]$ will miss the line segment $[(x_a,y_0),(x_b,y_0)]$, and therefore, for (x,y) on the line segment, this small ε range of angles will not contribute to $b(x,y)$ given by equation 2, and thus the $\tan^n\phi/\cos\phi$ singularity is avoided.

According to the theorem, testing the DCC for a parallel beam system can be achieved by simply performing a weighted backprojection onto a line segment outside the object, and verifying that the values on the line segment form a polynomial of the correct degree. The advantage of these DCC over the HL or other published conditions is that some projection truncation is allowed: only those lines which contribute to the backprojection $b_n(x,y_0)$ for $x_0 \in [x_a,x_b]$ are needed. In the simulations section below, we illustrate the large amount of projection truncation that can be sustained while still being able to check the DCC of the measurements.

Since the backprojection is only performed along a line segment rather than a 2D volume, the computational cost is very low. Furthermore, the number of points along taken along the line can be chosen to trade off between computational effort and the accuracy desired to check the polynomial. For our simulations (see below) we examined only orders $n = 0, 1, 2$ yet we chose about 100 points on the line segment.

For each backprojection of order n, a different weight is required. However, many different backprojections can be computed in parallel as only the weight depends on n.

III. An Illustration of DCC

A. Phantom and acquisition geometry

To illustrate the DCC we used a simple phantom made up of elliptical regions of constant density. Parallel beam projections of this phantom were obtained by computing exact line-lengths passing through the component ellipses. The phantom consists of a large elliptical shell of outer axes lengths 25 units x 40 units with several smaller elliptical features inside. The outer component of the elliptical shell is horizontally centered in the coordinate system but is displaced 10 units in the vertical direction (so its center is at (0,-10)). The phantom details are presented in Table 1, and Fig. 1 shows a sketch of it.

A non-truncated sinogram $p(\phi,r)$ was created of this phantom, for 1600 projections ϕ over the range $[-\pi/2, \pi/2)$ with 2560 samples for $r\in[-25,25]$. Also, a truncated sinogram $p^t(\phi,r)$ was considered which was the same as $p(\phi,r)$ by extracting the 1024 central samples for $r\in[-10,10]$ in each projection. This truncated sinogram corresponds to the field-of-view (FOV) of diameter 20 indicated in Fig. 1. The two sinograms are displayed in Fig 2. Note the heavy truncation of sinogram $p^t(\phi,r)$: every projection is truncated either on one side, or the other, or on both sides.

Table1: Ellipse Parameters

Ellipse	Center	(Dx, Dy)	Density
1a	(0, -10)	(40, 25)	0.5
1b	(0.5, -10)	(38, 24)	-0.5
2	(-5, -12)	(8.75, 8.75)	0.1
3	(2, -7)	(3.75, 2.5)	0.1
4	(4, 0)	(5, 2.5)	0.1
5	(-7, -1)	(1.25, 2.5)	0.1
6	(-3, 0)	(1.25, 1.25)	0.1
7	(-4, -4)	(2.5 2.5)	0.2
8	(-2, -3.5)	(1.5, 1.5)	0.2

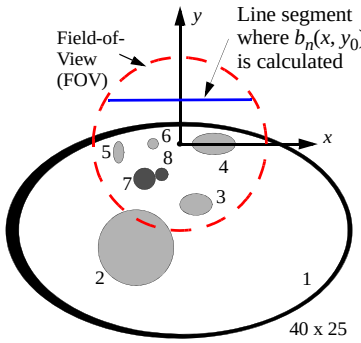

Fig 1. Illustration of the phantom, showing also the FOV corresponding to the truncated sinogram, and also the line-segment along which the backprojections were calculated for verifying data consistency.

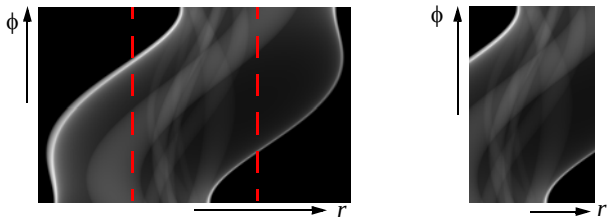

Fig 2. Sinograms. Left: the full 1600 projections (vertical axis) of 2560 elements each for large coverage of 50 units in diameter. The red lines show the boundary of the FOV indicated in Fig. 1. Right: the 1600 x 1024 truncated sinogram extracted from full sinogram, covering the 20 units diameter FOV shown in Fig 1.

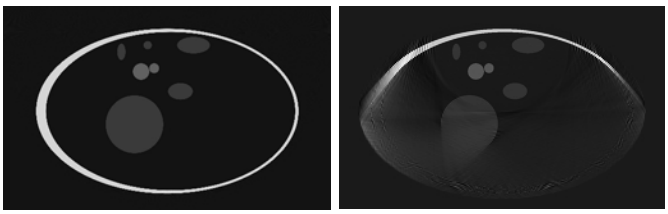

Fig 3. Reconstructions. Left: a FBP reconstruction of the full object from the full sinogram of Fig. 2. The reconstruction size was 1024 x 1024. Right: a conjugate gradient reconstruction from a downsampled 800 x 512 version of the truncated sinogram. The image size is 256 x 256. (Greyscale windows are not the same.)

Reconstructions from the two sinograms of Fig. 2 are shown in Fig. 3. From the full data, a standard filtered backprojection (FBP) reconstruction was performed. Accurate ("exact") ROI reconstruction from such truncated sinograms was only theoretically established in 2007 [Def07], but no suitable analytic reconstruction technique is known at this time. The image of Fig. 3 (right) was achieved by using a conjugate gradient method to minimize a least-squares criterion with a small amount of regularization. This ROI reconstruction from truncated data is computationally intensive.

B. Verifying data consistency conditions

From the simulated sinogram, the weighted backprojection functions $b_n(x, y_0)$ defined by equation 2 were calculated for the line segment $y = y_0$ with $y_0 = 5$ and $x \in [-8, 8]$ as illustrated in Fig. 1. We now drop the fixed y_0 and just write $b_n(x)$ for short. We only examined cases $n = 0, 1, 2$ and the backprojection was performed for 101 samples along the line segment, spaced every 0.16 units apart. The plots of Fig. 4 show least-squares fits of the backprojections b_n to polynomials of degree n. We note the excellent polynomial fits of the correct degree, as predicted by the theory.

The central observation here is that to perform the backprojections $b_n(x)$, only the truncated sinogram was necessary. All lines (sinogram entries) necessary to calculate the backprojection were available because the line-segment lies inside the FOV of Fig. 1. Thus we have found (and numerically verified) necessary DCC for the truncated sinogram $p^t(\phi, r)$.

IV. An Application of DCC

As an illustration of potential applications of truncated projection DCC, we consider a dynamic version of our phantom and illustrate how the DCC can be applied to search for 3 motion parameters.

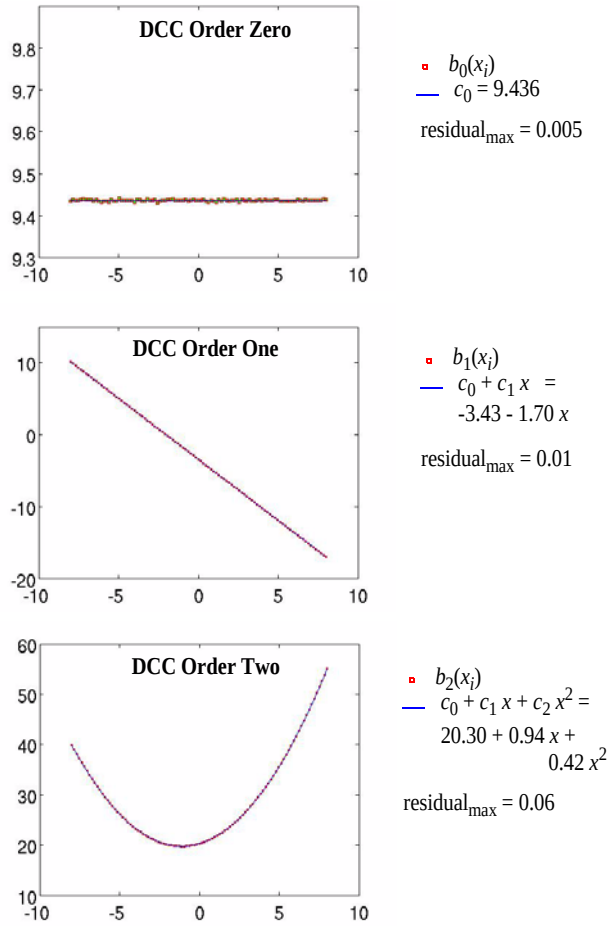

Fig 4. Data Consistency Conditions. The backprojections $b_0(x)$, $b_1(x)$, $b_2(x)$ were fit respectively to polynomials of degree 0, 1, 2. The three graphs show the original 101 values x_i along the line $x \in [-8, 8]$ and, superimposed, the best fit polynomial. The residual values are also listed.

A. Dynamic phantom

We define a dynamic version of the phantom which changes during the course of the scan and therefore the projections will not be consistent. The dynamic nature of the phantom is described by 3 nonlinear parameters, and the objective is to search for these parameters by minimizing inconsistency. For the dynamic phantom, ellipses 7 and 8 undergo a horizontal oscillatory motion (such as a tumour moving due to respiration). It is assumed that the shape and density of the "tumour" are known, but not the three motion parameters (t_0, t_1, A) defined below, and not the rest of the phantom.

We assume that the projections are gathered over T seconds uniformly, so $\phi_t = (\pi/T)t - \pi/2$. The centers of ellipses 7 and 8 are now $\Gamma_t(-4, -4)$ and $\Gamma_t(-2, -3.5)$ where

$$\Gamma_t(x, y) = \begin{cases} \left(x + \frac{A}{2} - \frac{A}{2}\cos\left(2\pi\frac{t - t_0}{t_1 - t_0}\right), y\right) & \text{if } t \in [t_0, t_1] \\ (x, y) & \text{otherwise} \end{cases} \quad (8)$$

For our simulation we use $T = 18$ seconds and $(t_0, t_1, A) = (2, 17, 7)$. Fig. 5 illustrates the motion.

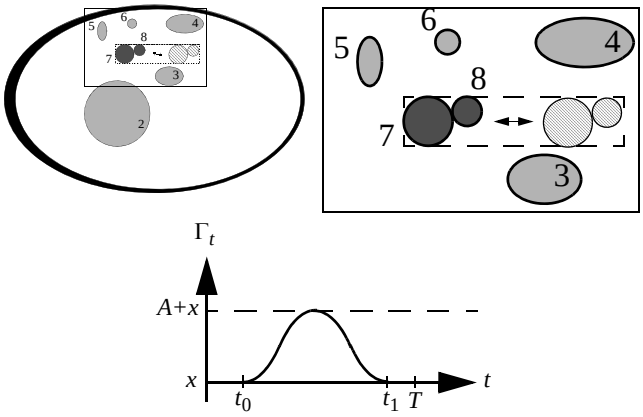

Fig 5. Dynamic Phantom details. Upper row: phantom and magnified insert illustrating horizontal motion of ellipses 7 and 8. Bottom: graph of the function Γ_t. The motion starts at t_0 and ends at initial position at t_1. The distance travelled in each direction is A.

B. Sinogram and reconstruction of dynamic data

As before, the (truncated) projections were simulated by using line-length calculations, but through the dynamic phantom described above. Fig. 6 shows the resulting sinogram and the reconstruction obtained from this sinogram. It is an interesting curiosity that the movement of disks 7 and 8 does not cause only a lateral blurring, but seems to suggest a triangular motion.

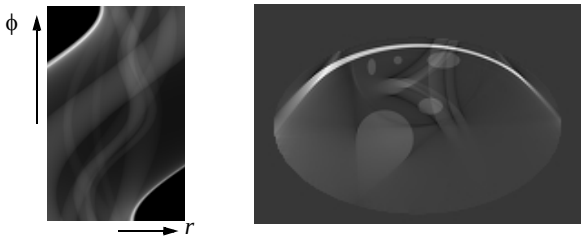

Fig 6. Left: sinogram p^{dyn} of the dynamic phantom, same parameters as in Fig. 2(right). Conjugate gradient reconstruction from the sinogram at left; same parameters as in Fig 3(right). Note that complicated blurring caused by motion.

C. Using DCC to identify the motion

We describe here our procedure for using DCC to estimate the three motion parameters of the tumour from the projections p^{dyn} of the dynamic phantom. We introduce non-negative cost functions $C_n(p)$ which are zero when the (truncated) sinogram is consistent. Recalling that b_n is the backprojection of p along the line segment, we define $C_n(p)$ to be the residual of the best degree-n polynomial fit to b_n. That is,

$$C_n(p) = \min_{q \in Q_n} \|q - b_n\|^2 \qquad (9)$$

where Q_n is the set of all polynomials of degree n.

Since we know the tumour properties, from a set of motion parameters (t_0, t_1, A) we can simulate its position at time t and thereby construct a simulated tumour sinogram $p^{\text{sim}}_{t_0, t_1, A}$. If we successfully estimate its motion parameters, they can be subtracted from the measurements p^{dyn} to give consistent data. So, we define a cost function $c(t_0, t_1, A)$ as follows:

$$c(t_0, t_1, A) = \sum_{n=1}^{2} C_n(p^{\text{dyn}} - p^{\text{sim}}_{t_0, t_1, A}) \qquad (10)$$

We used the Downhill Simplex method (see "amoeba" [Pre03]) to minimize $c(t_0, t_1, A)$ starting from four vertices of an initial simplex of (t_0, t_1, A) = (1.5, 16, 6), (3, 16, 6), (1.5, 17.5, 6), (1.5, 16, 7.5) with respective costs 0.27, 0.88, 0.31, 0.63. We obtained, after 204 evaluations of the cost function, the values $(\tilde{t_0}, \tilde{t_1}, \tilde{A})$ = (1.98, 16.99, 7.03) with a cost of 0.19 (which was slightly lower than the cost at the "true" motion parameters (t_0^*, t_1^*, A^*) = (2, 17, 7)).

In Fig. 7 we show the sinogram $p^{\text{sim}}_{\tilde{t_0}, \tilde{t_1}, \tilde{A}}$ of the estimated movement of the tumour, which we subtract from the measured sinogram p^{dyn} to give a corrected sinogram $p^{\text{dyn}} - p^{\text{sim}}_{\tilde{t_0}, \tilde{t_1}, \tilde{A}}$ which is the most consistent possible according to our procedure. We performed a motion-corrected reconstruction from this consistent sinogram, and in comparing with Fig. 6 we note that the motion artifacts have been virtually eliminated.

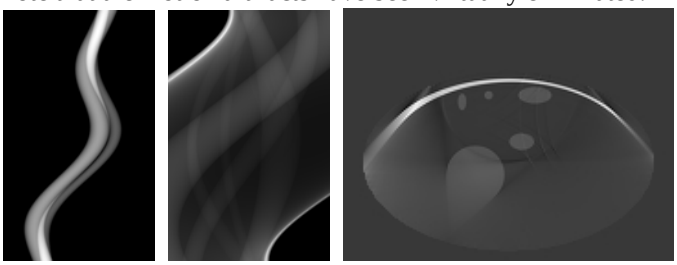

Fig 7. Motion correction by DCC. Left: DCC estimated motion $p^{\text{sim}}_{\tilde{t_0}, \tilde{t_1}, \tilde{A}}$ in measured sinogram p^{dyn}. Center: Sinogram after motion component has been subtracted: $p^{\text{dyn}} - p^{\text{sim}}_{\tilde{t_0}, \tilde{t_1}, \tilde{A}}$. Right: Reconstruction obtained from corrected sinogram, showing dramatically reduced motion artifacts (compare to Fig. 6).

V. Discussion and Conclusions

We have derived necessary DCC for truncated parallel projections. We believe these to be the first published DCC for truncated projections. The conditions were applied to a toy problem in motion estimation and compensation to illustrate their potential for practical applications.

DCC for truncated *fanbeam* projections are possible using the same principles as shown here, but the backprojection step would be more elaborate, probably requiring 2D interpolations.

The backprojection weight functions are closely related to expressions appearing in recently-published fanbeam DCC [Cla13]. The link can be seen by considering the virtual fanbeam approach (see [Cla10] for a description) applied to the truncated parallel projections.

VI. References

[Agu95] V. Aguilar and P. Kuchment. "Range conditions for the multi-dimensional exponential x-ray transform." *Inv. Probs* 11, 977-982, 1995.

[Bas00] S. Basu and Y. Bresler. "Uniqueness of tomography with unknown view angles." *IEEE Trans Imag Proc* 9, 1092-1106, 2000.

[Che05] G.-H. Chen and S. Leng. "A new data consistency condition for fan-beam projection data." *Med Phys* 32, 961-967, 2005.

[Cla10] R. Clackdoyle and M. Defrise. "Tomographic Reconstruction in the 21st Century: Region-of-interest reconstruction from incomplete data." *IEEE Sig Proc Mag.* 27, 60-80, 2010.

[Cla13] R. Clackdoyle. “Necessary and Sufficient Consistency Conditions for Fanbeam Projections along a Line.” *IEEE Trans Nucl Sci*, 60, 1560-1569, 2013.

[ClD13] R. Clackdoyle and L. Desbat. “Full data consistency conditions for cone-beam projections with sources on a plane.” *Phys. Med. Biol*. 58, 8437-8456, 2013.

[Def03] M. Defrise, F. Noo, and H. Kudo. “Improved two-dimensional rebinning of helical cone-beam computerized tomography data using Johns equation.” *Inv. Probs* 19, S41-S54, 2003.

[Def06] M. Defrise, F. Noo, R. Clackdoyle, and H. Kudo. “Truncated Hilbert transform and image reconstruction from limited tomographic data” *Inv. Probs* 22,1037-1053, 2006.

[Edh86] P.R. Edholm, R.M. Lewitt and B. Lindholm. “Novel properties of the Fourier decomposition of the sinogram.” *Proc SPIE* 671, 8-18, 2006.

[Fin83] D.V. Finch and D.C. Solmon. “Sums of homogeneous function and the range of the divergent beam X-ray transform.” *Numer Func Anal and Optimiz* 5, 363–419, 1983.

[Hel80] S. Helgason. *The Radon Transform*. (Boston: Birkhauser), 1980.

[Hsi04] J. Hsieh, E. Chao, J. Thibault, B. Grekowicz, A. Horst, S. McOlash and T.J. Myers. “A novel reconstruction algorithm to extend the CT scan field-of-view.” *Med. Phys*. 31, 2385–2391, 2004.

[Joh38] F. John. “The ultrahyperbolic differential equation with four independent variables.” *Duke Math. J*. 4, 300-322, 1938.

[Lev10] M.S. Levine, E.Y. Sidky and X. Pan. “Consistency Conditions for Cone-Beam CT Data Acquired with a Straight-Line Source Trajectory.” *Tsinghua Sci Technol* 15, 56–61, 2010.

[Lud66] D. Ludwig. “The Radon transform on Euclidean space.” *Comm. Pure Appl. Math.* 19, 49–81, 1966.

[Maz10] S.R. Mazin and N.J. Pelc. “Fourier properties of the fanbeam sinogram.” *Med. Phys* 37, 1674-1680, 2010.

[Nat83] F. Natterer. “Computerized tomography with unknown sources.” *SIAM J. Appl. Math*. 43, 1201-1212, 1983.

[Pat02] S.K. Patch. “Consistency conditions upon 3D CT data and the wave equation.” *Phys. Med. Biol*. 47, 2637-2650, 2002.

[Pre03] W.H. Press, S.A. Teukolsky, W.T. Vetterling, B.P. Flannery. *Numerical Recipes in C++* (Cambridge: Masson) 2003.

[Tan11] S. Tang, X. Mou, Q. Xu, Y. Zhang, J. Bennett and H. Yu. “Data consistency condition-based beam-hardening correction.” *Opt. Eng.* 50, 076501(1–13), 2011.

[Yu06] H. Yu, Y. Wei, J. Hsieh and G. Wang. “Data Consistency Based Translational Motion Artifact Reduction in Fan-Beam CT.” *IEEE Trans. Med. Imag*.25, 792–803, 2006.

[Yu07] H. Yu and G. Wang. “Data Consistency Based Rigid Motion Artifact Reduction in Fan-Beam CT.” *IEEE Trans. Med. Imag*. 26, 249–260, 2007.